Bulk anisotropy embedded in fault gouges and shear fabrics

Eomzi Yang[1], S.H., Hyun[1], and T.S. Yun[1]

[1] Department of Civil and Environmental Engineering, Yonsei University, Yonsei-ro 50, Seoul, South Korea.

ABSTRACT

The weak strength of fault rocks should be considered for assessing the stability of infrastructure near fault zone and the weak strength is originated from the discontinuities, and fabric orientation of fault rocks. The previous studies of the embedded anisotropy in fault rock are usually based on 2D analysis, for example, the thin section method, so that the procedure requires much time and extensive workload. In this study, we propose a statistical method called 'Slicing Plane Method (SPM)' which gives the major anisotropy induced by its structure. Also, it is confirmed that the anisotropy of structure is related to the reduction in the shear strength of fault gouge.

Keywords: Slicing Plane Method, Fault gouge, Anisotropy

1 INTRODUCTION

The shear fabric in the fault zone is highly correlated with the tectonic movement of geological formation as an evidence of shear movement from micro- to macro-scales (Tchalenko, 1970; Rutter et al., 1986). The strain states evolved in the fault zone have been evaluated by morphological features of shear fabric, corroborated by the field observations (Chester and Logan, 1986; Bullock et al., 2015). These fabrics construct the planar anisotropy of the fault gouge so that the orientation is interpreted as a foliation, discontinuity of fault zone (Chester and Logan, 1987). It is shown that the weak strength of fault core, the inner part of fault zone which accommodates most fault slip, is related to the composition and fabric orientation of gouge (Niemejier et al., 2010; Lockner et al., 2011). It suggests that the characterization for the anisotropy of fault zone is crucial to assess geo-mechanical stability of the surrounding area near the fault zone. The previous studies have primarily examined the anisotropy embedded in the fault zone as a consequence of shear movement by either two-dimensional visual inspections or indirect non-destructive methods (Chester and Logan, 1987; Cladouhos, 1999; Haines et al., 2009). However, the anisotropy in fault gouge is originated from the spatial configuration of constituents so that the three-dimensional observation is prerequisite to assess how each component in the fault gouge is contributory to the bulk anisotropy. The internal structure of fault zone can be associated with the characterization of rock mass because several rock mass classifications include the parameters similar to the anisotropy induced by the discontinuities of rock mass. RMR takes into account the orientation of discontinuity of rock mass with respect to the excavation direction for tunneling and GSI has been developed for the determination of rock mass properties, extending to the complex sheared rock mass (Bieniawski, 1989; Hoek and Brown, 1997; Hoek et al., 1998). These classifications are also based on expert-dependent surface observation so that it is necessary for methods to quantify the 3D spatial information for more comprehensive understanding of the anisotropy in fault core. In this study, we apply the statistical method called 'Slicing Plane Method (SPM)' that process spatial variation of materials based on X-ray CT grayscale number (Yun et al. 2013). The SPM gives the direction that grayscale number most varies and the resulted stereo-net implies the periodicity of the variation of materials. The visual observation of 2D sliced images reveals that grains in natural fault gouge is not proper to be used as a marker of shear movement in fault zone. For 3D analysis, we segment the embedded fracture, grains and matrix

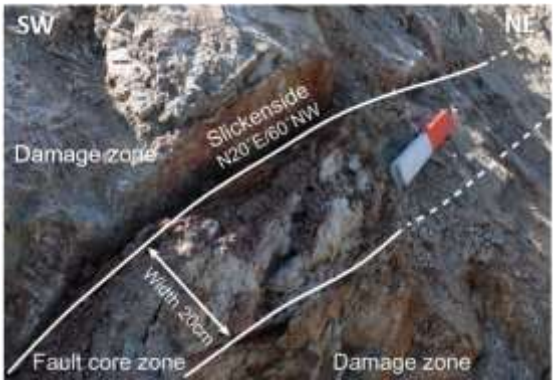

Fig 1. Field observation at Yecheon Shear Zone

depending on the gray-scale values followed by the SPM analysis. The results show that the bulk anisotropy is mainly attributed to the layered structure composed of fracture planes or matrix parallel to the fault zone boundary.

2 MATERIALS & METHOD

2.1 Geological setting

The fault zone exists within 20 km from Yecheon Shear Zone, the ductile strike-slip zone in South Korea. The slickenside next to the fault core run along N 20°E and 60°NW (Fig.1).

2.2 Data acquisition

The specimens are cored in three directions orthogonal to each other. Each direction is defined as the axis of the coordinate system in this study; x-direction is perpendicular to the fault plane, y-direction is parallel to the strike of the fault plane, and z-direction is orthogonal to xy-plane. Total 27 specimens are cored with diameter of 80 mm and height of 30 mm. Three specimens are subjected to 3D X-ray CT imaging with the resolution of less than 80 μm. The rest is used for direct simple shear test (ASTM D 3080).

2.3 Method

The SPM defines the directional vector and the corresponding normal plane. The imaginary normal plane slices 3D image of the specimen and the average of gray-scale values on the plane (μ_g) are calculated. The slicing plane moves along the given directional vector followed by computing μ_g. After calculating μ_g for a given direction, the coefficient of variation (c_v) is defined as

$$c_v = \frac{\sigma^{\mu_g}}{\mu^{\mu_g}} \quad (1)$$

$\sigma^{\mu g}$ is standard deviation of the set of μ_g, and $\mu^{\mu g}$ is average of μ_g. Finally, c_v means the normalized intensity of grayscale number variation. For entire directions, the prescribed procedures are repeated and the orientation having the maximum c_v naturally indicates the major anisotropy in the bulk specimen. Fig 2 shows the results of SPM when the anisotropy of layered structure is normal to z-direction. The contrast of Domain I is more intense than that of Domain II and the periodic interval of Domain I is shorter than that of Domain III. The stereo-net plot resulted from SPM exhibit similar trend to the above. Maximum c_v of Domain I is higher than that of Domain II and the range of nonzero is more concentrated to the z axis than Domain III.

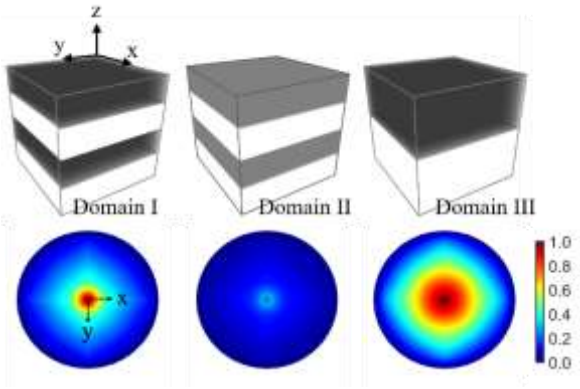

Fig 2. Ideal domain for Slicing Plane Method

3 RESULTS

3.1 The orientation of grain

The X-ray CT of fault gouge shows the embedded grains with their fragmented shape. The green arrow in Fig. 3a recalls that y-direction is parallel to the strike of the fault plane. The specimen cored along z-direction shows that grains have equant shape while the grains with nonequant shape are fractured. It is observed that some grains have cracks subparallel to y-direction and their relative positions are maintained. This implies that the external stress state was developed after the formation of fault zone as the grains are ruptured (Fig. 3a). The specimen cored along x-direction shows the apparent fault plane parallel to y-direction. Some grains are fractured with the crack subparallel to y-direction but it appears that grains are much more shattered than the above (Fig .3b). It is difficult to consider that there is any anisotropy of the orientation of grains or shape of grains. This suggests that the orientation of grains in fault gouge have little relationship with the shear movement in fault zone because the consequential shape of grains from the formation of fault zone is dependent up on the initial shape of grains and their compositions as well as the external stress state.

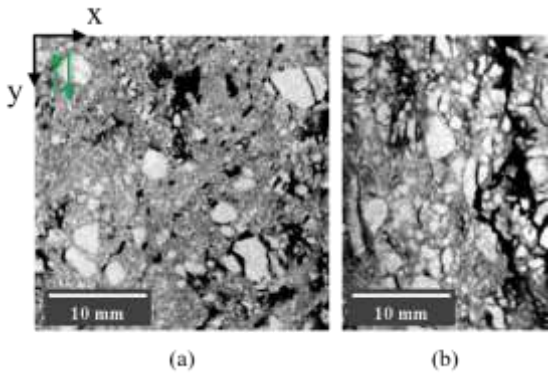

Fig 3. X-ray CT image of fault gouge (a) specimen cored along z-direction (b) specimen cored along x-direction

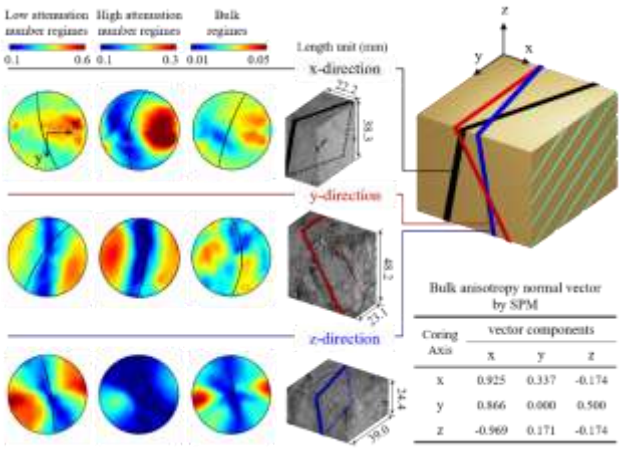

Fig 4. Result of SPM for matrix and fracture of specimens

3.2 The orientation matrix and fracture

The reliability of SPM has been verified by characterizing the anisotropy of Mudstone, Sandstone, Gneiss, and Granite (Yun et al., 2013). It showed that SPM is quite independent to the effect of image resolution, ring artifact and scattered beam hardening.

The X-ray attenuation number reflects the relative density of materials consisting of specimens and the gray value of X-ray CT image represents each constituent. Low attenuation number regimes below assigned threshold value can be set as the fracture or void regime and the rest corresponding to relatively higher attenuation number matches to matrix and grain regime.

We apply SPM to fracture network by binarizing low attenuation number regime. As the domain data is binary, the intensity of c_v is higher than that of high attenuation regime and bulk regime (Fig. 4). The great circles on stereonet plots mean the plane normal to the directional vector of maximum c_v, and represents the plane parallel to major anisotropy of the specimens. The great circles of fracture regime are subparallel to y-direction within 30°. The periodic interval of fracture network of specimen cored along x-direction is shorter than that of specimens cored along other direction.

The regimes with high attenuation number corresponding to grains and matrix of specimens have great circles more parallel to y-direction. The specimen cored along x-direction shows the most intense anisotropy. On the other hands, the specimen cored along z-direction has the shortest periodic interval though the intensity of anisotropy is lowest. It seems reasonable to consider as the anisotropy of high attenuation number regime is mainly controlled by matrix because grains have little anisotropy as stated earlier.

The stereonet plots in the third column of Fig. 4 show the bulk anisotropy of each specimen. Compared with the stereonets of both segmented regimes, the orientation of great circles is governed by the orientation of high attenuation number regime associated with the matrix anisotropy. This is because SPM calculate c_v based on the corresponding area of the slicing plane. The number of pixels of matrix and grains is significantly higher than that of fracture network so that the orientation of bulk anisotropy is determined close to the orientation of matrix anisotropy. The great circles are rotated within a range of 30° in azimuth and 20° in elevation. This means that the bulk anisotropy is developed almost parallel to the strike of fault plane. X-ray CT images with slicing plane in the fourth column presents the relationship between spatial variation of grayscale numbers and the bulk anisotropy of the specimen. This is reorganized on the virtual 3D domain. The greenish lines on the face of cube means the slickensides determined from the field observation. The fault plane defined by the slickensides is subparallel to the great circles of the bulk anisotropy.

The range of c_v for bulk anisotropy is over 0.01-0.05 which is 3-6 times higher compared with the results of SPM for Berea sandstone which has discontinuity by bedding plane (Jeong, 2018). It suggests that natural fault gouge has meaningful anisotropy without selecting certain indicator such as Riedel shear, P-foliation and shape of grains (Chester and Logan, 1986; Cladouhos, 1999).

3.3 The anisotropy of shear strength

We conducted the direct simple shear tests of 24 specimens in four directions to understand the effect of bulk anisotropy in fault gouge. Remolding of specimens to match the shearing plane and the orientation of bulk anisotropy can cause severe disturbance. Direction I-1 is equal to the strike of the fault plane. Direction I-2 is perpendicular to the strike of the fault plane but still is on the fault plane. Direction II is perpendicular to both the fault plane and its strike. Direction III is perpendicular to the fault plane but parallel to the strike of the fault plane. Simply, Direction I-1, I-2 is parallel to the fault plane and Direction II, III is perpendicular to the fault plane (Fig 5). The normal stress of 54.0, 107.9, 161.9 kPa are applied for each specimen with the horizontal displacement rate less than 1mm/min under ASTM D 3080-98. The load cell measures the horizontal force every 1 sec until the displacement reaches 15% of the specimen diameter.

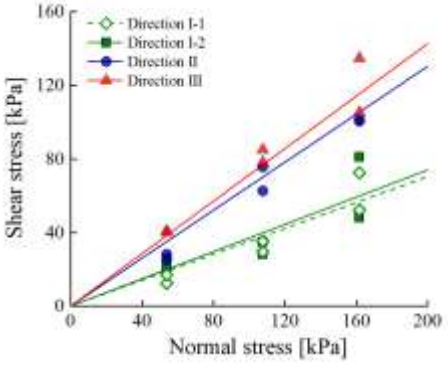

Fig 5. Results of direct simple shear test

The friction angle is determined by Mohr - Coulomb's failure criteria. The friction angle of Direction I-1, I-2, II, and III is 19.4º, 20.3 º, 33.1 º, and 35.5 º, respectively. The friction angles of Direction I-1, I-2 is much lower than that of Direction II, III. It suggests that the shear strength of fault gouge drops when the orientation of fault plane and the shearing direction is parallel. The previous studies reported that the difference in compositions of fault gouge results in the descrepancy of shear strength (Collettini et al., 2011; Kato and Hirono, 2016). This study proposes that the anisotropy of shear strength can be caused by the structural anisotropy as well as the effect of the mineralogy in fault gouge.

4 CONCLUSION

In this study, we employ SPM for the characterization of the anisotropy in fault gouge.

- Natural fault gouge has apparent bulk anisotropy which can be considered as the structural anisotropy.
- Grains in fault gouge barely contribute to the structural anisotropy or the estimation of the shear movement in fault zone.
- The bulk anisotropy of natural fault gouge is majorly controlled by the anisotropy of matrix.
- It is observed that the anisotropy of structure in fault gouge results in the anisotropy of shear strength.

ACKNOWLEDGEMENTS

This work was supported by the National Research Foundation of Korea (NRF) grant funded by the Korea government (MSIP) (No.2016R1A2B4011292) and the Land and Housing Institute (LHI) grant funded by the Korea Land and Housing Corporation.

REFERENCES

Bieniawski, Z.T., 1989, Engineering rock mass classifications: a complete manual for engineers and geologists in mining, civil, and petroleum engineering: New York, Wiley, xii, 251

Bullock, R.J., Paola, N.D. and Holdsworth, R.E. (2015) An experimental investigation into the role of phyllosilicate content on earthquake propagation during seismic slip in carbonate faults, Journal of Geophysical Research, 120(5), 3187-3207

Cladouhos, T.T. (1999) Shape preferred orientations of survivor grains in fault gouge, Journal of Structural Geology, 21(4), 419-436

Chester, F.M., and Logan, J.M. (1986) Implications for mechanical properties of brittle faults from observations of the Punchbowl fault zone, California, Pure Applied Geophysics, 124(1), 79-106

Chester, F.M., and Logan, J.M. (1987) Composite planar fabric of gouge from the Punchbowi Fault, California, Journal of Structural Geology, 9(5/6), 621-634

Collettini, C., Niemeijer, A., Viti, C., Smith, S. A. F., and Marone, C. (2011) Fault structure, frictional properties and mixed-mode fault slip behavior. Earth and Planetary Science Letters, 311(3), 316–327, https://doi.org/https://doi.org/10.1016/j.epsl.2011.09.020

Haines, S.H., van der Pluijm, B.A., Ikari, M.J., Saffer, D.M. and Marone, C. (2009) Clay fabric intensity in natural and artificial fault gouges: Implications for brittle fault zone processes and sedimentary basin clay fabric evolution, Journal of Geophysical Research, 114(B5)

Hoek, E., and Brown, E.T., 1997, Practical estimates of rock mass strength: International Journal of Rock Mechanics & Mining Sciences, v. 34, p. 1165-1186

Hoek, E., Marinos, P., and Benissi, M., 1998, Applicability of the Geological Strength Index (GSI) classification for very weak and sheared rock masses. The case of the Athens Schist Formation: Bulletin of Engineering Geology and the Environment v. 57, p. 151-160

Jeong, Y.J., (2018) Evaluation of long-term stability and storage efficiency of reservoir rocks considering anisotropic features in CO2 geological sequestration (Doctoral dissertation, Yonsei Unviersity, Seoul, Korea)

Kato, N. and Hirono, T. (2016) Heterogeneity in friction strength of an active fault by incorporation of fragments of the surrounding host rock, Earth, Planets and Space, 68(1), 134, https://doi.org/10.1186/s40623-016-0512-3

Lockner, D. A., C. Morrow, D. Moore, and S. Hickman (2011), Low strength of deep San Andreas fault gouge from SAFOD core, Nature, 472(7341), 82-85, doi: 10.1038/nature09927

Niemeijer, A., C. Marone, and D. Elsworth (2010), Fabric induced weakness of tectonic faults, Geophys. Res. Lett., 37(3), L03304, doi: 10.1029/2009GL041689

Rutter, E.H., Maddock, R.H., Hall, S.H. and White, S.H. (1986) Comparative Microstructures of Natural and Experimentally Produced Clay-Bearing Fault Gouges, Pure Applied Geophysics, 124(1-2), 3-30

Tchelenko, J.S. (1970) Similarities between Shear Zone of Different Magnitudes, Geological Society of America Bulletin, 81, 1625-1640

Yun, T.S., Jeong, Y.J., Kim, K.Y., Min, K.B. (2013) Evaluation of rock anisotropy using 3D X-ray computed tomography, Engineering Geology, 163, 11-19